Prediction of the dynamic response of composite sandwich beams under shock loading

V.L. Tagarielli, V.S. Deshpande and N.A. Fleck[1]

Cambridge University Engineering Dept.
Trumpington St., Cambridge, CB2 1PZ, UK

Abstract

Finite element calculations are reported for the dynamic shock response of fully clamped monolithic and sandwich beams, with elastic face sheets and a compressible elastic-plastic core. Predictions of the peak mid-span deflection and deflected shape of the beam are compared with the previously reported measured response of end-clamped sandwich beams, made from face sheets of glass fibre reinforced vinyl ester and a core of PVC foam or balsa wood (Tagarielli V.L., Deshpande V.S. and Fleck N.A.. *The dynamic response of composite sandwich beams to transverse impact*, Int. J. of Solids and Structures, 44, 2007) [1]. Good agreement is observed, and the maximum sustainable impulse is also predicted adequately upon assuming a tensile failure criterion for the face sheets. The finite element calculations can also be used to bound the response by considering the extremes of a fully intact core and a fully damaged core. It is concluded that the shock resistance of a composite sandwich beam is maximised by selecting a composite with fibres of high failure strain.

Keywords: composite sandwich, FE, cellular solid, dynamic loading, blast resistance

Submitted to International Journal of Impact Engineering, October 2008

[1] Corresponding author: Tel. +44(0)1223 748240; Fax. +44(0)1223 332662 E-mail: naf1@eng.cam.ac.uk

1 INTRODUCTION

Sandwich panels comprising composite face sheets and a lightweight core, such as polymer foams or balsa wood, are extensively employed in marine structures as they provide superior quasi-static bending stiffness and strength to monolithic beams. The quasi-static flexural response of these structures has been investigated by a number of authors (see for example Steeves and Fleck [2],[3] and Tagarielli et al. [4]) for several loading and boundary conditions, and is now adequately understood. It is generally appreciated that the static response of a sandwich structure can outperform that of a monolithic structure of equal mass.

A significant body of literature exists on the experimental characterisation of composite sandwich plates subject to low-velocity transverse impact. In this regime, inertial effects are negligible and the deformation and failure mechanisms are the same as those obtained for quasi-static loading, see for example Abrate [5], Shubel et al. [6] and Zenkert et al. [7]. A number of analytical models for the low-velocity impact of sandwich beams and plates have been developed (e.g. Librescu et al. [8], Perel and Palazzotto [9], Li et al. [10]). These models are inappropriate for the case of intense dynamic loading for at least one of the following reasons:

1. They assume that the dynamic modes of deformation are identical to the quasi-static modes.
2. They employ linear, small-deflection plate theory and thereby neglect the dominant contribution of face sheet and core stretching upon the structural response.
3. They ignore plastic core compression in the transverse direction, and they do not account for failure.

At higher impact velocities inertial effects become important, and the deformation and failure modes can differ substantially from those observed in a quasi-static scenario.

The blast resistance of sandwich structures to intense underwater explosions is of obvious concern in military applications. Analytical and numerical models suggest that metallic sandwich structures outperform metallic monolithic structures under fluid-shock loadings (Fleck and Deshpande [11], Xue and Hutchinson [12]). These predictions have been verified by more detailed calculations and accompanying sets of

experiments. Much less is known about the blast response of composite sandwich structures.

Tagarielli et al. [1] have measured the dynamic response of end-clamped sandwich beams made from face sheets of glass fibre reinforced vinylester and a core of PVC foam or balsa wood. The beams were loaded transversely at mid-span using metal foam projectiles. Upon impact the projectiles exerted a pressure pulse of about 100 MPa for a duration of approximately 0.1 ms. This loading technique was introduced by Radford et al. [13] for simulating blast loading on a sandwich structure, and was used by Radford et al. [14] and Rathbun et al. [15] to measure the dynamic response of metallic sandwich beams with lattice cores. Tagarielli et al. [1] found that a composite sandwich beam deflects much less then a monolithic beam of the same mass.

In the experimental study by Tagarielli et al. [1], the composite sandwich beams were loaded by metal foam projectiles travelling at high speed, and the deflection versus time history of the structure was recorded via high-speed photography. The observed deformation mechanism comprised propagation of a transient flexural wave along the beam, accompanied by stretching. The failure modes were explored as a function of imposed impulse and sandwich geometry, and included fibre tearing, core cracking and interfacial delamination.

The phenomena investigated are sufficiently complex that a combination of numerical analysis and experiments is required. Other authors have relied solely on computation. For example, Bahei-El-Din et al. [16] have performed finite element simulations of the blast response of a composite sandwich beam with composite faces and a PVC foam core. They argued that the addition of a polyurea interlayer enhanced the blast resistance. In order to gain confidence into the set of assumptions underlying their simulations, instrumented tests are required.

In the present study, finite element simulations are performed to help interpret the observations of Tagarielli et al. [1]. The simulations also serve to validate recently developed constitutive descriptions (Deshpande and Fleck [17], Tagarielli et al. [18]) for the PVC foam and balsa wood cores.

1.1 Scope of study

First, a brief summary of the main experimental findings of Tagarielli et al. [1] is reported for end-clamped composite sandwich beams subjected to transverse loading at mid-span by metal foam projectiles. The results of this previous experimental investigation motivate our numerical analysis.

Second, explicit finite element calculations are performed for the dynamic response of fully clamped monolithic and sandwich beams, with elastic face sheets and a compressible elastic-plastic core. A visco-plastic formulation is employed for the PVC foam and balsa wood cores, based upon the multi-axial constitutive descriptions of Deshpande and Fleck [19] and Tagarielli et al. [18]. The rate sensitivity of the core materials is taken from the independent measurements of Tagarielli et al. [20]. Finally, the FE predictions are compared with the observed response, including the maximum admissible blast impulse assuming a tensile failure criterion for the face sheets.

2 SUMMARY OF MEASURED DYNAMIC RESPONSE OF COMPOSITE SANDWICH BEAMS

Tagarielli et al. [1] have measured the response of end-clamped composite monolithic and sandwich beams to dynamic transverse loading. The beams were impacted transversely by circular cylindrical projectiles made from an aluminium alloy foam of density $\rho_p = 350\,\mathrm{kgm}^{-3}$ (i.e. relative density 13%). The projectiles of length $L_p = 36\,\mathrm{mm}$, diameter $D_p = 28.5$ mm (and mass $m_p = \pi D_p^2 L_p \rho_p = 0.008\,\mathrm{kg}$) were fired at a velocity v_p in the range of 50 ms^{-1} to 400 ms^{-1}. Both ends of the beam were fully clamped, as sketched in Fig. 1. The geometry of the beam and the relevant material properties for the face sheets and the core are also defined in Fig. 1.

The sandwich beams comprised composite face sheets and a foam core. The face sheets were made from a laminated stack of four plies of lay-up $[0, \pm 45, 90]$ or eight plies of symmetric lay-up $[0, \pm 45, 90]_S$. The dry fibres were infiltrated with vinyl ester resin and were bonded to the core in a single step by cold vacuum infusion. The overall density

of the composite faces was approximately 1700 kg m^{-3}. Three types of foam core were used, each supplied by DIAB[2] :
(i) H100 Divinycell PVC foam (density 100 kgm^{-3}),
(ii) H250 Divinycell PVC foam (density 250 kgm^{-3}) and
(iii) an end-grain balsa wood (DIAB designation ProBalsa LD7, density 90 kgm^{-3}), with the cell direction aligned with the thickness direction of the core.

For each core material, sandwich beams were manufactured with a range of face sheet and core thicknesses but with a fixed span of $2L$ = 200 mm and width b = 30 mm. The face sheet and core thickness were chosen in order to obtain three target values of areal mass m of sandwich beam. Monolithic beams were also manufactured from the quasi-isotropic glass-vinylester composites to achieve the same areal mass as that of the sandwich beams. The ten geometries of monolithic and sandwich beams tested by Tagarielli et al. [1] are summarised in Table 1. Monolithic beams are designated with the letter M while the sandwich beams with a core made from the low density H100 PVC, the high density H250 PVC and Balsa wood are denoted by the letters H, HD and B, respectively. The specimens have been arranged in the table to form sets of equal areal mass: Set 0 is for a single monolithic beam, while Sets 1 to 3 comprise monolithic and sandwich beams.

The mid-span deflection versus time history of the monolithic and sandwich beams was measured by high speed photography. Deformation was by the propagation of elastic flexural waves along the beam, accompanied by a string-mode retardation and finally arrest. Significant springback occurred such that the residual deformation was negligible in most cases. The maximum mid-span deflection of the beam increased with increasing projectile momentum, and the observed failure modes were core fracture (CF), face sheet debonding (D), and face sheet tearing (FT), as sketched in Fig. 2. It was found that catastrophic failure of the beam was by face sheet tearing. The reference case of an intact core will be denoted by (IC) in this paper.

The peak back-face, mid-span deflection W is plotted in Fig. 3 against the initial areal momentum $I_0 = \rho_p L_p v_p$ of the projectile, for the monolithic and sandwich beams. Each

[2] DIAB AB, Box 201, 312 22 Laholm – Sweden.

curve is for a single geometry and is a best-fit through the experimental data of the previous study. Typically, 3 to 6 tests were performed for each geometry over a range of I_0. The data points are omitted for the sake of clarity, and the line style for each curve is chosen to collect together the responses for Sets 1 to 3 of Table 1. The curves in Fig. 3 were truncated at the impulse for which ultimate failure was observed by Tagarielli et al. [1]. We note that W increases with I_0 but there is no straightforward dependence of W upon the areal mass m or the beam composition. The following detailed finite element calculations are needed in order to interpret these results.

3 FINITE ELEMENT CALCULATIONS

Finite element (FE) simulations have been performed in order to develop an understanding for the dynamic modes of deformation of composite sandwich beams, and to compare directly with the observed deformation histories reported by Tagarielli et al. [1].

Two-dimensional (2D) plane strain dynamic calculations were performed using the general-purpose finite element package ABAQUS Explicit (HKS - *Hibbitt, Karlsson & Sorensen, Inc.*). In the plane strain calculations, the circular projectile was replaced by a rectangular projectile of length L_p, density ρ_p and cross-sectional area equivalent to that of the circular cylindrical projectile such that the equivalent projectile was taken to have a rectangular cross-section of width b and span 2a with $2ba = \pi D_p^2 / 4$. In all experiments in Tagarielli et al. [1] we have $D_p = 28.5$ mm and b = 30 mm, giving an equivalent projectile span of $2a = 21.3$ mm. The projectile, of mass m_p and initial velocity v_p, is initially in contact with the beam. The geometry and material properties of the beams and projectile were taken to be consistent with the experimental investigation of Tagarielli et al. [1]. Selected three-dimensional calculations have also been performed to justify the use of the much simpler 2D approach, see Appendix A for this comparison.

Plane strain 4-noded rectangular elements were employed, of type CPE4R in the ABAQUS notation, for both the sandwich beam and the metal foam projectile. Only

half of the beam was modelled due to symmetry, and the clamped boundary conditions were enforced by constraining horizontal and vertical motion of all nodes at the ends of the beam, as sketched in Fig. 1. Typically elements with a maximum edge length of 1 mm were used to model the sandwich and monolithic beams. The prescription used to specify the mesh in the foam projectile is detailed in Section 3.3.

3.1 Constitutive description of the face sheets

Tagarielli et al. [1] performed uniaxial tension and compression tests on the composite face sheets, at a strain rate of 10^{-4} s^{-1}. The face sheets were linear elastic to failure in both tension and compression. It is assumed that the modulus of the glass fibre composite is independent of strain rate. The density ρ_f, axial Young's modulus E_f, in-plane Poisson's ratio ν_f, tensile strength σ_T and micro-buckling strength σ_C are summarized in Table 2 for each thickness of face sheet.

In the finite element simulations, the monolithic beams and the face sheets of composite sandwich beams were treated as elastic isotropic solids. This approximation is justified by the fact that the dominant stress state within the face sheets is uniaxial bending and stretching; through-thickness stresses within the face sheets are small and have a negligible effect upon the overall response. This idealisation of face sheet behaviour has been used previously to model the static response of composite sandwich beams with face sheets made from a quasi-isotropic stack of composite plies (see Steeves and Fleck [3], Tagarielli et al. [4]).

3.2 Constitutive description of the cores

PVC foam cores

Both quasi-static and dynamic compressive tests were performed by Tagarielli et al. [20] on the H100 and H250 PVC foam cores. Results from these tests are used in the present study to calibrate the constitutive models for the PVC foam core. Preliminary checks revealed that the PVC foams were isotropic. Uniaxial compression tests were performed

on the PVC foams at strain rates in the range 10^{-4} to 10^{4} s^{-1}. The loading direction was chosen to be normal to the face of the core in the sandwich plate configuration. At all strain rates employed, the stress versus strain response had an initial elastic regime followed by a plastic plateau at almost constant stress, and densification at a nominal strain ε_D.

Tagarielli et al [20] found that the compressive plateau stress σ_{pl} for the PVC foams scales with the applied strain rate $\dot{\varepsilon}$ according to the power law relation

$$\sigma_{pl} = \sigma_0 \left(\frac{\dot{\varepsilon}}{\dot{\varepsilon}_0^{pl}} \right)^N \tag{1}$$

Values of σ_0 and N (with the reference strain rate chosen to be $\dot{\varepsilon}_0^{pl} = 1$ s^{-1}), along with the density ρ, modulus E, densification strain ε_D and Poisson's ratio ν are listed in Table 3 for the foams.

The PVC foams were modelled as a compressible, isotropic visco-plastic solid. A creep potential was derived from the yield surface of Deshpande and Fleck [19] for polymeric foams. This yield surface comprises the inner envelope of an ellipsoid and flat facets in principal stress space, and assumes that compressive yield is governed by a maximum principal stress criterion. The physical basis for this modification is that polymeric foams collapse by elastic buckling of the cell walls under macroscopic compression. First, we summarise briefly the rate-independent case of Deshpande and Fleck [19], and then we state the visco-plastic version.

Write Y and $Y_C = Y/\beta$ as the respective uniaxial tensile and compressive yield strengths of the PVC foam. Here σ_e is the von Mises stress and σ_m is the mean (or hydrostatic) stress. The ellipsoidal yield surface is defined via an overall equivalent stress measure $\hat{\sigma}$

$$\hat{\sigma}^2 \equiv \frac{1}{1+(\alpha/3)^2}(\sigma_e^2 + \alpha^2 \sigma_m^2) \le Y^2 \tag{2}$$

The material constant α defines the aspect ratio of this yield surface, and for PVC foams we take $\alpha = 2.12$. The equivalent plastic strain rate $\dot{\hat{\varepsilon}}$ is the work conjugate of $\hat{\sigma}$ and

can be expressed in terms of the von Mises effective strain rate $\dot{\varepsilon}_e$ and the volumetric plastic strain rate $\dot{\varepsilon}_{\mathrm{m}}$ according to

$$\dot{\bar{\varepsilon}}^2 = \left(1+\left(\alpha/3\right)^2\right)\left(\dot{\varepsilon}_{\mathrm{e}}^2 + \alpha^{-2}\dot{\varepsilon}_{\mathrm{m}}^2\right) \tag{3}$$

where

$$\dot{\varepsilon}_{\mathrm{e}}^2 \equiv \frac{2}{3}\dot{\varepsilon}_{ij}^{\mathrm{pl}}\dot{\varepsilon}_{ij}^{\mathrm{pl}} \quad \text{and} \quad \dot{\varepsilon}_{\mathrm{m}} \equiv \dot{\varepsilon}_{ii}^{\mathrm{pl}}$$

upon adopting the usual Einstein summation convention for repeated suffixes. Finally, the flat facets of the yield surface for PVC foams, in principal stress space $\left(\sigma_{\mathrm{I}}, \sigma_{\mathrm{II}}, \sigma_{\mathrm{III}}\right)$ are given by

$$\sigma_{\mathrm{I}} \geq -Y_{\mathrm{C}}; \quad \sigma_{\mathrm{II}} \geq -Y_{\mathrm{C}}; \quad \sigma_{\mathrm{III}} \geq -Y_{\mathrm{C}} \tag{4}$$

A visco-plastic description is adopted in the present study, with the plastic strain rate $\dot{\varepsilon}_{ij}^{pl}$ derived from a creep potential $\Phi\left(\sigma_{ij}\right)$ such that

$$\dot{\varepsilon}_{ij}^{pl} = \frac{\partial \Phi}{\partial \sigma_{ij}} \tag{5}$$

This potential is written as

$$\Phi\left(\sigma\right) = \Phi_I + \Phi_{II} + \Phi_{III} + \Phi_E \tag{6}$$

where

$$\Phi_i = \frac{N\sigma_0\dot{\varepsilon}_0^{pl}}{N+1}\left(\frac{\left|\sigma_i\right|}{\sigma_0}\right)^{\frac{N+1}{N}} H\left(-\sigma_i\right) \quad , \quad i = I, II, III,$$

and

$$\Phi_E = \frac{N\beta\sigma_0\dot{\varepsilon}_0^{pl}}{N+1}\left(\frac{\hat{\sigma}}{\beta\sigma_0}\right)^{\frac{N+1}{N}} \tag{7}$$

in terms of the material constants (σ_0, N, β) and the Heaviside step function $H(\cdot)$. For the case of uniaxial tensile loading with a stress σ, the creep law follows as

$$\dot{\varepsilon}^{\mathrm{pl}} = \dot{\varepsilon}_0^{\mathrm{pl}}\left(\frac{\sigma}{\sigma_0}\right)^{\frac{1}{N}} \tag{8}$$

In contrast, when the foam is subjected to a uniaxial compressive stress σ, the uniaxial plastic strain rate is the sum of two contributions,

$$\dot{\varepsilon}^{\mathrm{pl}} = -\dot{\varepsilon}_0^{\mathrm{pl}} \left(\frac{|\sigma|}{\sigma_0} \right)^{\frac{1}{N}} - \dot{\varepsilon}_0^{\mathrm{pl}} \left(\frac{|\sigma|}{\beta\sigma_0} \right)^{\frac{1}{N}} \tag{9}$$

The creep parameters (σ_0, N) for the PVC foams have been measured by Tagarielli et al. [20] and are listed in Table 3 (with the reference strain rate chosen to be $\dot{\varepsilon}_0^{\,pl} = 1\mathrm{s}^{-1}$); for both the H100 and H250 PVC foams we have $\beta = 1.5$.

Lock-up at densification is included in the analysis by enforcing an elastic response when any of the principal strain values ε_I^{pl} attains the densification strain ε_D, as given in Table 3.

Balsa wood core

The static and dynamic material responses of the balsa wood were measured by Tagarielli et al. ([18],[20]). Uniaxial compression and single-lap shear tests were performed in the in-plane and transverse directions of the balsa wood sheets and revealed that the balsa wood has a plastically compressible, transversely isotropic response.

In the finite element simulations the balsa core is treated as a rate dependent, transversely isotropic compressible solid. Choose the Cartesian axes of reference (x_1, x_2, x_3) such that the axes $x_1 - x_2$ lies in the isotropic plane and x_3 is along the grain (recall that in the dynamic sandwich beam experiments of Tagarielli et al. [1], the x_3 core direction is aligned with the axis of the cylindrical projectile, as indicated in Fig. 1). The rate-dependent plastic response is based upon the equivalent stress $\bar{\sigma}$ for a transversely isotropic compressible solid,

$$\begin{aligned} &\bar{\sigma}^2 \equiv B^2(\sigma_{11}^2 + \sigma_{22}^2) + \sigma_{33}^2 - C^2\sigma_{11}\sigma_{22} + \\ &-D^2\sigma_{33}(\sigma_{11} + \sigma_{22}) + E^2\sigma_{12}^2 + F^2(\sigma_{32}^2 + \sigma_{13}^2) = \sigma_0^2 \end{aligned} \tag{10}$$

as discussed by Tagarielli et al. [18]. The five constants B to F characterise the degree of plastic anisotropy of the balsa core, and are listed in Table 4 from the measurements of Tagarielli et al. [18]. The elastic response is also transversely isotropic and the elastic constants are included in Table 4, again from Tagarielli et al. [18].

A visco-plastic version was implemented in the finite element simulations, again based on a creep potential $\Phi(\sigma_{ij})$, where

$$\Phi(\bar{\sigma}) = \frac{N\sigma_0 \dot{\varepsilon}_0^{pl}}{N+1}\left(\frac{\bar{\sigma}}{\sigma_0}\right)^{\frac{N+1}{N}} \tag{11}$$

in terms of (σ_0, N). The values for (σ_0, N) are taken from Tagarielli et al. [20] and are listed in Table 3 for the choice $\dot{\varepsilon}_0^{pl}$=1 s^{-1} . Lock-up at densification is included in the analysis by enforcing an elastic response when $\bar{\varepsilon}^{pl}$ (work-conjugate to $\bar{\sigma}$) attains the densification strain ε_D, as given in Table 3.

3.3 Constitutive description of the metal foam projectiles

The metal foam projectile was treated as a rate-dependent compressible solid using the Deshpande and Fleck [17] constitutive law. The yield and hardening properties of the metal foam were calibrated using uniaxial compression data of Alporas foam specimens (Radford et al. [13]).

Subsequent to impact, a plastic shock wave travels along the axis of the projectile. In order to capture the propagation of this plastic shock-wave in a robust computational manner, strain rate sensitivity is introduced in the form of an overstress, linearly viscous model as

$$Y\left(\hat{\varepsilon}^{pl}\right) = Y_0 + \mu\dot{\hat{\varepsilon}} \tag{12}$$

Here, Y is the current yield stress, $\dot{\hat{\varepsilon}}$ is the effective plastic strain rate as defined in eq. (3), and μ is an artificial viscosity. $Y_0(\hat{\varepsilon})$ is the quasi-static compressive stress versus strain response oft the foam. It is adequately represented by a perfectly plastic characteristic of flow strength $Y_0 = 2.1$ MPa up to a nominal densification strain of 0.8. An elastic response is assumed post-densification. A viscosity of $\mu = 225$ Pa$\cdot$s and element size of $e = 0.1$ mm were adequate to resolve the plastic shock wave in the metal foam, as discussed by Deshpande and Fleck [21].

4 ACCURACY OF THE FINITE ELEMENT PREDICTIONS

4.1 Deformation history of the sandwich beams

In the experimental study of Tagarielli et al. [1], high speed photographs were obtained for each dynamic experiment on the composite sandwich beams listed in Table 1. In this study, comparisons were made between the FE-predicted and observed deformation histories of each sandwich beam. As an example, consider the beam HD1, impacted at mid-span by a metal foam projectile of mass 0.008 kg travelling at a velocity of 96 ms^{-1}.

The right-hand side of Figure 4 (a)-(g) contains a sequence of frames with the deformation history of the beam after impact, as predicted by FE. The deflected profile of the bottom face sheet, as observed by Tagarielli et al. [1] or predicted by FE simulations, are shown in the left-hand side of Fig. 4 (a)-(g). It is clear that a good qualitative and quantitative agreement is found between experiment and FE simulation.

The time history of mid-span deflection of the bottom face of the beam, $w(t)$, is given in Fig. 4 (h); again, the measured and predicted responses are shown. The frames in Fig. 4 (a)-(g) correspond to the points marked in Fig. 4 (h). The two curves in Fig. 4 (h) are qualitatively similar but present some discrepancies. Nevertheless, it is evident that the FE simulation captures accurately both the maximum deflection of the sandwich beam and the response time, defined as the time required for the beam to achieve maximum mid-span deflection.

We proceed by exploring the accuracy of the FE predictions for all the geometries in Table 1 and for a range of impact velocities. The most convenient way to make the comparison is to plot the maximum non-dimensional back-face, mid-span deflection $\bar{W} = W / L$ as a function of the applied impulse (projectile momentum) per unit area, as quantified by the non-dimensional parameter $\bar{I} = I_0 / \left(L\sqrt{\rho_f E_f} \right)$, ρ_f and E_f are the density and the Young's modulus of the composite face sheets (or of the monolithic beam), respectively. The mass of the beam is represented by the non-dimensional parameter $\bar{M} = m / m_0$, where m is the areal mass of the beam and the reference value

m_0 is the areal mass of the monolithic beam M1 (M1 constitutes Set 0 in Table 1). The above choice of non-dimensionalisation of I_0 follows that employed by Fleck and Deshpande [11], upon replacing the strength of the face sheet by its modulus E_f.

4.2 Maximum deflection versus applied impulse: monolithic beams

Figure 5 shows the measured peak mid-span deflection $\overline{W}$ as a function of the applied impulse per unit mass, as quantified by $\hat{I} = \overline{I} / \overline{M}$, for the clamped monolithic beams M1 and M2. The choice $\hat{I}$ is appropriate for beams which absorb their kinetic energy mainly by axial, elastic stretching rather than by bending. The measured values display significant scatter and Tagarielli et al. [1] associated this with the observed variability in modulus. A re-analysis of our original data revealed that the thin monolithic beams had an initial deflection of $\overline{W} \approx 0.02$ upon tightening of the test fixture. This problem only arose for the case of the monolithic beams as their bending stiffness is much less than that of the sandwich beams.

Now consider the finite element predictions for the maximum deflection of the composite beams. The predictions are included in Fig. 5 and are in broad agreement with the measurements, subject to the above caveats on the experimental data. It is clear from Fig. 5 that $\overline{W}$ is a unique function of $\hat{I}$ for both beams: this supports the notion that the beams are deflecting primarily by elastic stretching. The vertical arrows and label FT in the figure denote the impulse at which catastrophic failure is observed by face tearing. The measured peak deflection $\overline{W}$ is then arbitrary and for definiteness we place the experimental data points on the FE predictions.

4.3 Maximum mid-span deflection versus applied impulse: sandwich beams

Sandwich beams with a H250 PVC foam core

Figure 6 presents experimental results and FE predictions for sandwich beams with a H250 PVC foam core. Figures 6 (a), (b) and (c) relate to the beam configurations HD1, HD2 and HD3, respectively. As indicated in the figures by the IC label, no core fracture was observed in the dynamic experiments on sandwich beams with a H250 PVC foam core. Consequently, the FE predictions are adequate.

Sandwich beams with a H100 PVC foam core

Figure 7 contains a comparison of measured and predicted $\bar{W}$ for clamped sandwich beams with a H100 PVC foam core. Results are shown in parts (a), (b) and (c) for the sandwich beams H1, H2 and H3, respectively. The labels IC, CF and CFD denote the observed mode of core failure while FT denotes again ultimate failure by face sheet tearing, as defined in Fig. 2. We emphasize that these three beams have markedly different areal masses, as already noted in Table 1.

The agreement between experiments and predictions is adequate for configurations H1 and H2 (Figs. 7 (a) and (b)), but $\bar{W}$ is underpredicted for configuration H3. Note that the beam H3 suffers core fracture accompanied by face sheet delamination (CFD). In contrast, the configuration H2 undergoes only core fracture (CF) at large $\bar{I}$. It is concluded that face sheet delamination leads to a dramatic increase in peak deflection $\bar{W}$, and this is not captured by the present FE simulations. To explore this further, we performed an additional set of FE predictions for the sandwich beam H3 upon neglecting the presence of the core.

The sandwich beam is now replaced by a monolithic beam of thickness twice that of the sandwich face sheet. This idealisation mimics the major drop in bending stiffness of the sandwich beam and the minor drop in axial stiffness due to debonding of the core. The FE predictions for this monolithic beam are now in good agreement with the observed peak deflections of the sandwich beam H3.

Sandwich beams with a balsa wood core

The results from dynamic experiments conducted on balsa wood core sandwich beams are reported in Fig. 8, along with the FE predictions. Figures 8 (a) and (b) present results for the specimens B1 and B2, respectively. Each of these figures includes the response of the monolithic beam M1 for comparison: this monolithic beam is identical to beams B1 and B2, absent the core. For beams B1 and B2, core cracking and face sheet delamination was observed at all levels of applied impulse.

The finite element predictions are in good agreement with the measurements, despite the fact that the sandwich beams have undergone delamination. This is in sharp contrast to the case of sandwich beams with a H100 PVC core, as detailed above. This has been traced to the feature that the balsa wood has a lower shear strength than the H100 PVC foam and undergoes shear yielding in the simulations. Consequently, the face sheets of the sandwich beam with an intact balsa core behave similarly to two independent monolithic beams, with negligible overall sandwich action. These independent face sheets are slender and deform mainly by stretching. By this argument, a doubled-up face sheet in the form of the monolithic beam M1 will still deform predominantly by stretching and will have similar deflections to those of the sandwich with an intact balsa core. The comparable deflections for beams M1, B1 and B2 support this argument. The measured response of the failed sandwich beams are close to the predictions for the sandwich beams with an intact balsa core.

5 FAILURE PREDICTION OF SANDWICH BEAMS

Tagarielli et al. [1] have made approximate measurements of the required impulse in order to cause tearing of the sandwich beams. In all cases, catastrophic failure was by face sheet tearing. The observed failure impulse is bounded by two measured values, namely the impulse at which perforation is observed in the test, and a lower applied impulse for which negligible face tearing occurs. These two levels of impulse give upper and lower limits on the failure impulse.

The FE simulations of the current study were used to predict face sheet failure as follows. The longitudinal strains in the composite faces, averaged over the cross-section

of the face sheets, were extracted from the simulations as a function of time. It was found that the average strain was a maximum at the built-in ends of the front face sheet, for all sandwich beam geometries. The time at which the maximum strain is attained coincides with the time at which the beam reaches its maximum deflection. Similarly, for monolithic beams, the maximum strain is attained at the encastre section when the beam reaches the maximum deflection.

Figure 9 (a) presents FE predictions of the maximum strain attained in the beam as a function of the applied non-dimensional impulse, for two representative beams: the monolithic beam M2 and the sandwich beam H3. We assume that face sheets fail when the maximum longitudinal strain attains the static failure strain of 2.5%, as observed by Tagarielli et al. [1]. This failure criterion is used in order to predict the maximum impulse that can be sustained by beams without perforation. For the beams M2 and H3, the maximum impulse is given by the cross-symbols in Fig. 9 (a). The figure includes the measured lower and upper limits of failure impulse. The agreement between the measured and predicted failure impulse is satisfactory for these two structures.

In Fig. 9 (b) the failure impulse predicted by the FE simulations is compared to the measured values for all the monolithic and sandwich beams of Table 1. For most of the beam geometries, good agreement is noted. In contrast, the FE predictions under-predict the failure impulse for the sandwich geometries HD1, HD2, HD3 and H2. No explanation can be provided as to why these four structures were much more resistant to perforation than predicted. In broad terms, our predictions give the initiation of failure and do not account for damage development. Thus, the predictions are somewhat conservative.

6 CONCLUDING REMARKS

This study has focused on the dynamic response of clamped monolithic and sandwich beams comprising composite face sheets and a lightweight core. Dynamic finite element simulations have been performed to predict the maximum mid-span deflection of monolithic and sandwich beams as a function of the applied impulse.

With an appropriate choice and calibration of the constitutive models for the core material, FE simulations are able to predict correctly the dynamic response of clamped sandwich beams to shock loading over a central patch.

Core fracture may have a minor effect upon the dynamic response of sandwich beams. In contrast, face sheet debonding dramatically impairs the dynamic performance of composite sandwich beams, and as a result the core ductility and the toughness of the bonding interface are key parameters in the design of a sandwich beams for dynamic strength. It remains to develop satisfactory FE approaches which include modelling of damage initiation and evolution.

The ultimate failure of the sandwich beams is by face sheet tearing, and can be predicted conservatively by a maximum principal strain failure criterion. It follows that the dynamic shock resistance of the composite sandwich beams can be maximised by selecting face sheet materials with a high failure strain.

APPENDIX A: Justification of the 2D FE approach: results for 2D and 3D simulations

In the majority of this study, two-dimensional (2D) FE simulations are used to predict the dynamic response of the clamped beams. In this section, we justify this simplification.

The FE calculations performed in this study attempt to mimic the experiments in Tagarielli et al. [1], in which prismatic composite beams were impacted by circular cylindrical metal foam projectiles. Thus, the problem is three-dimensional (3D) in nature, and a set of 3D simulations are required. However, 3D FE calculations are much slower than 2D calculations, and a set of 2D and 3D calculations were performed to demonstrate that a 2D model suffices.

In the 2D, plane strain calculations, the circular projectile was replaced by a rectangular projectile of length L_p, density ρ_p and cross-sectional area equivalent to that of the circular cylindrical projectile. Assume that the beam is of width b. Then, the equivalent projectile was taken to have a rectangular cross-section of width b and span 2a such that $2ba = \pi D_p^2 / 4$. In all experiments in Tagarielli et al. [1] we have D_p = 28.5 mm and b = 30 mm, giving an equivalent projectile span of $2a$ = 21.3 mm.

In order to verify the equivalence of the two calculations, selected 2D and 3D simulations were performed, and their results compared. A single clamped monolithic beam, and a single clamped sandwich beam with high density PVC foam core have been considered, corresponding to the specimens M2 and HD2 of Table 1.

In the 3D calculations, 8-noded brick elements of type C3D8R were used, and the simulations were performed by modelling in detail the impact of a circular cylindrical projectile of length L_p = 40 mm and mass $m_p = 0.008$ kg as used in the experimental investigation. The simulations were performed using two values of impact velocity. The results are presented in Fig. A1 as plots of the non-dimensional mid-span back-face deflection $\overline{w} = w / L$ versus the non-dimensional time $\overline{t} = t / L\sqrt{\rho_f / E_f}$, where ρ_f and E_f

are the face sheet density and Young's modulus, respectively. For both the monolithic and sandwich beams results are compared for the 2D and 3D simulations. It is clear from Fig. A1 (a) that the 2D and 3D calculations give very similar results for the monolithic beam. However, the 2D calculation gives a slightly stiffer response than the 3D simulation for the sandwich beam, see Fig. A1(b). Despite this small discrepancy, we limit our attention to 2D plane strain simulations throughout this study.

REFERENCES

[1] Tagarielli V.L., Deshpande V.S. and Fleck N.A., 2007. *The dynamic response of composite sandwich beams to transverse impact*, Int. J. of Solids and Structures, 44.

[2] Steeves C.A. and Fleck N.A., 2004a. *Collapse mechanisms of sandwich beams with composite faces and a foam core, loaded in three-point bending. Part I: analytical models and minimum weight design.* International Journal of Mechanical Science, 46:561-583.

[3] Steeves C.A. and Fleck N.A., 2004b. *Collapse mechanisms of sandwich beams with composite faces and a foam core, loaded in three-point bending. Part II: experimental investigation and numerical modelling*. Int. J. Mechanical Sciences, 46(4), 585-608.

[4] Tagarielli V.L., Fleck N.A. and Deshpande V.S., 2004b. *Collapse of clamped and simply supported composite sandwich beams in three-point bending*, Composites B: Engineering, 35, 523–534.

[5] Abrate S., 1998. *Impact on composite structures,* Cambridge University Press.

[6] Shubel P.M., Luo J.-J. and Daniel, 2005. *Low velocity impact behaviour of composite sandwich panels.* Composites: Part A. 36: 1389-1396.

[7] Zenkert D., Shipsha A., Bull P. and Hayman B., 2005. *Damage tolerance assessment of composite sandwich panels with localised damage.* Composite Science and Technology, 65: 2597-2611.

[8] Librescu L., Oh S.Y. and Hohe J., 2004. Linear and non-linear dynamic response of sandwich panels to blast loading. Composites: Part B, 35:673-683.

[9] Perel V.Y. and Palazzotto A.N., 2003. *Dynamic geometrically nonlinear analysis of transversely compressible sandwich panels,* Int. Jou. of Nonlinear Mech., 38: 337-356.

[10] Li Q.M., Ma G.W. and Ye Z.Q., 2006. *An elastic-plastic model on the dynamic response of composite sandwich beams subjected to mass impact,* Composite Structures, 72: 1-9.

[11] Fleck N.A. and Deshpande V.S., 2004. *The resistance of clamped sandwich beams to shock loading*, J. of Applied Mechanics, ASME, 71:386-401.

[12] Xue Z. and Hutchinson J. W., 2003. *A Comparative Study of Blast-Resistant Metal Sandwich Plates*, to appear in Int. J. Impact Eng.

[13] Radford D.D., Deshpande V.S., Fleck N.A., 2004a. *The use of metal foam projectiles to simulate impulse loading on a structure*. To appear in J. Impact Engineering.

[14] Radford D. D., Fleck N. A. and Deshpande V. S., 2004b. *The response of clamped sandwich beams subjected to shock loading*, to appear in Int. J. of Impact. Eng.

[15] Rathbun H.J., Radford D.D., Xue Z., He M.Y., Yang J., Deshpande V.S., Fleck N.A., Hutchinson J.W., Zok F.W. and Evans A.G., 2004. *A dynamic probe for validating simulations of shock loaded metallic sandwich panels*, to appear in Int. J. of Solids and Structures.

[16] Bahei-El-Din Y.A., Dvorak G.J. and Fredricksen O.J., 2006. *A blast-tolerant sandwich plate design with a polyurea interlayer*. Int. J. of Solids and Structures**,** Volume 43, Issues 25-26, 7644-7658.

[17] Deshpande V.S. and Fleck N.A., 2000. *Isotropic constitutive models for metallic foams*. J. Mech. Phys. Solids; 48, 1253-1283.

[18] Tagarielli, Deshpande, Fleck and Chen, 2004a. *A transversely isotropic model for foams, and its application to the indentation of balsa*, to appear in Int. J. Mech. Sci.

[19] Deshpande V.S. and Fleck N.A., 2001. *Multiaxial yield behaviour of polymer foams*. Acta Materialia; 49, 1859–1866.

[20] Tagarielli V.L., Deshpande V.S. and Fleck N.A., 2008. *The high strain rate response of PVC foams and end-grain balsa wood,* to appear in Composites Part B: Engineering.

[21] Deshpande VS, Fleck NA., 2004. *One-dimensional shock response of sandwich beams.* To appear in J. Mech. Phys. Solids.

FIGURE CAPTIONS

Fig. 1. (a) Geometry of a fully clamped sandwich beam impacted centrally by a metal foam projectile. Schematisation of the full FE simulations conducted in this study.

Fig. 2. Sketches of the dynamic failure modes of composite sandwich beams, observed by Tagarielli et al. [1].

Fig. 3. Summary of the observed peak deflections versus applied impulse, for the beams in Sets 1, 2 and 3 in Table 1.

Fig. 4. (a)-(g) Deformation history of the sandwich beam HD1 impacted by a metal foam projectile. The back-face deflection profile is reported on the left hand side, as predicted by an FE simulation or extracted from high-speed photographs. The deformation of the beam predicted by a FE simulation is presented on the right hand side. (h) Measured and predicted mid-span deflection of the bottom face sheet as a function of time.

Fig. 5. Maximum mid-span deflection of the clamped monolithic beams M1 and M2 as a function of the non-dimensional applied impulse (normalised by the non-dimensional mass of the beam). Experiments are compared with FE simulations. The occurrence of tearing is indicated by the symbols FT and the vertical arrows.

Fig. 6. Maximum mid-span deflection as a function of the applied impulse for sandwich beams with a H250 core, of type (a) HD1, (b) HD2 and (c) HD3. Experimental results are compared with FE predictions. The observed damage and failure modes are denoted by IC and FT.

Fig. 7. Maximum mid-span deflection as a function of the applied impulse for sandwich beams with a H100 core, of type (a) H1, (b) H2 and (c) H3. Experimental results are compared with FE predictions. The observed damage and failure modes are denoted by IC, CF, CFD, FT. Figure 7 (c) includes FE predictions for a clamped monolithic beam of axial stiffness approximately equal to that of the sandwich beam H3.

Fig. 8. Maximum mid-span deflection as a function of the applied impulse for sandwich beams with a balsa wood core, of type (a) B1, (b) B2. Experimental results are compared with FE predictions. The observed damage and failure modes are denoted by CFD, FT. In both (a) and (b), FE predictions for the monolithic beam M1 have been included for comparison.

Fig. 9. (a) FE predictions of the maximum strain attained in the monolithic beam M2 and in the face sheets of the sandwich beam H3, as a function of the non-dimensional applied impulse. Observed failure impulse intervals for these two structures are included in the figure. (b) Comparison of observed and FE-predicted non-dimensional failure impulse for all the monolithic and sandwich specimens listed in Table 1.

Fig. A1. Non-dimensional mid-span deflection versus time history for (a) the monolithic beam M2 and (b) the sandwich beam HD2, impacted by a metal foam projectile at selected projectile velocities. Results from two- and three-dimensional FE simulations are compared.

TABLE CAPTIONS

Table 1: The geometry of the sandwich beams tested by Tagarielli et al. [1]. The specimens labelled M denote monolithic beams, H and HD denote sandwich beams with the H100 and H250 PVC foam cores, respectively, and the specimens labelled B are the sandwich beams with a balsa wood core. The specimens are divided into 4 sets, with beams in each set having approximately equal areal masses (indicated in the Table). The span for all beams tested was $2L = 200\,\text{mm}$, and the width $b = 30\text{mm}$.

Table 2: The mechanical properties of the woven GFRP/Vinylester face sheets tested by Tagarielli et al. [1]. Material parameters are listed for two values of the sheet thickness.

Table 3: Summary of the mechanical properties of the three core materials tested by Tagarielli et al. [20].

Table 4. Additional material data for the balsa wood core.

	Beam designation	Face sheet thickness *h*, mm	Core thickness *c*, mm
Set 0, $m \approx$ 2.5 kgm^{-2}	M1	1.5	monolithic
Set 1, $m \approx$ 3.5 kgm^{-2}	M2	2.2	monolithic
	H1	0.85	5
	B1	0.85	5
Set 2, $m \approx$ 4.3 kgm^{-2}	H2	0.85	15
	HD1	0.85	5
	B2	0.85	15
Set 3, $m \approx$ 6.3 kgm^{-2}	H3	1.5	10
	HD2	0.85	15
	HD3	1.5	5

Table 1

thickness	ρ, kgm^{-3}	E, GPa	ν	σ_T, MPa	σ_C, MPa
h = 0.85 mm	1700	9	0.25	220	145
h = 1.5 mm or 2.2 mm	1700	14	0.25	340	225

Table 2

	ρ, kgm^{-3}	E, MPa	ν	compressive strength, MPa	ε_D	σ_0, MPa	N
H100	100	125	0.25	1.7	-1.6	1.95	0.016
H250	250	400	0.25	5.8	-1.4	7.44	0.047
Balsa	90	1850	0.25	4.5	-1.6	5.87	0.055

Table 3

Elastic properties	$E_{33} = 1850$ MPa; $E_{11} = 300$ MPa; $G_{13} = 700$ MPa; $\nu_{12} = 0.2$; $\nu_{13} = 0.1$
Plastic properties	$B^2 = 54$; $C^2 = D^2 = 0$; $E^2 = 484$; $F^2 = 30$

Table 4

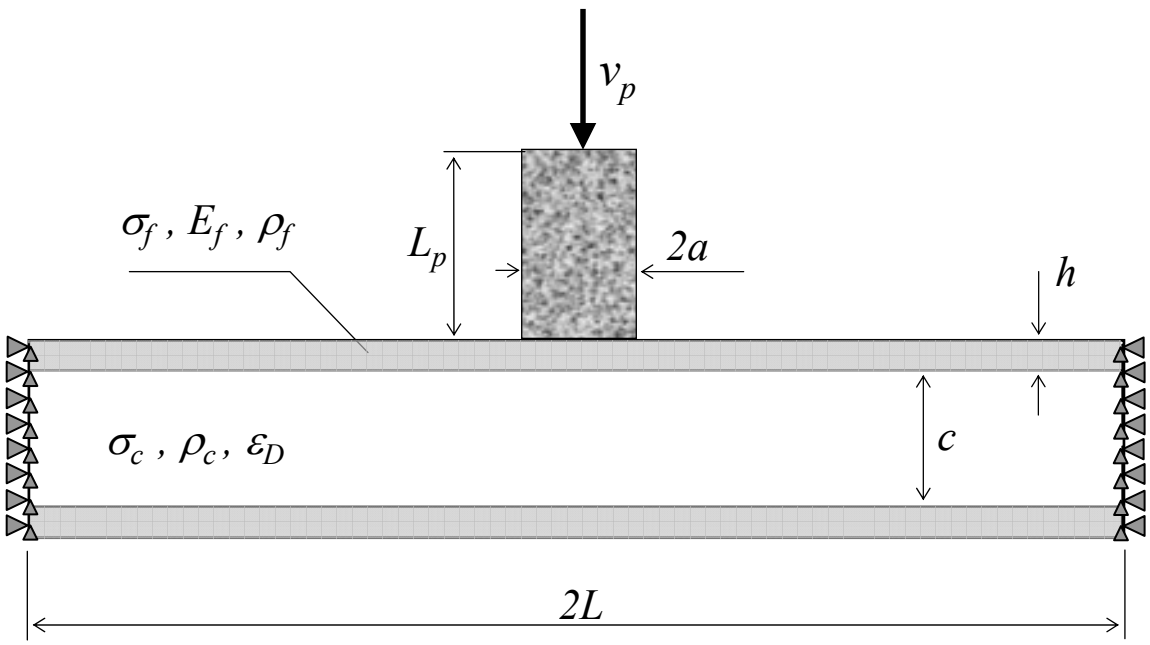

Fig. 1

CF: *core fracture*

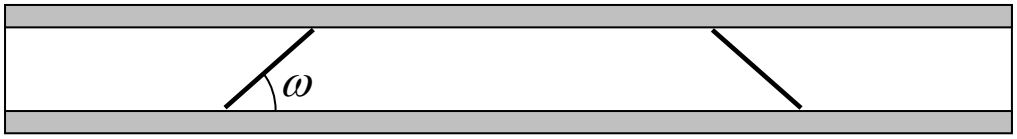

CFD: *core fracture* + *debonding*

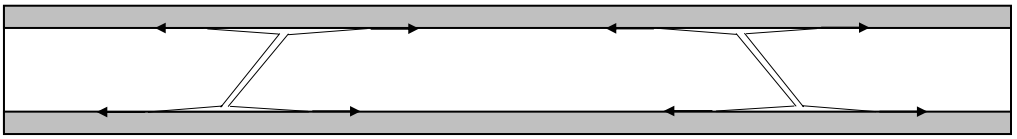

FT: *face sheet tearing*

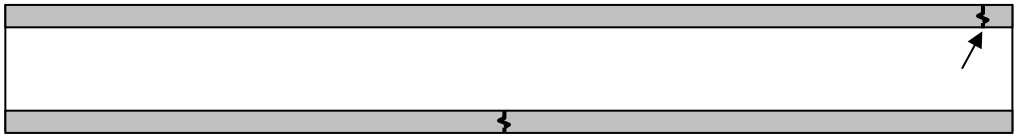

Fig. 2

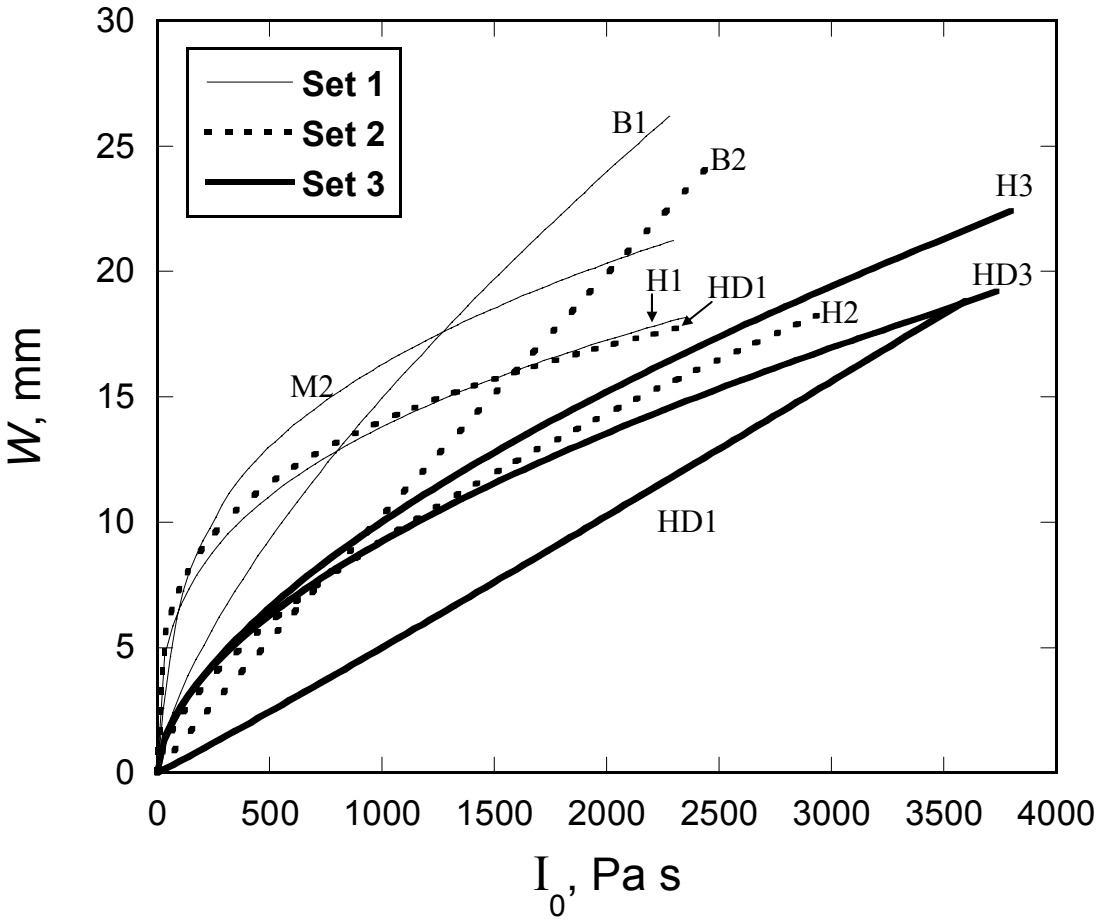
Set 1
Set 2
Set 3
B1
B2
H3
H1
HD1
HD3
H2
M2
HD1
W, mm
I0, Pa s
0
5
10
15
20
25
30
0
500
1000
1500
2000
2500
3000
3500
4000

Fig. 3

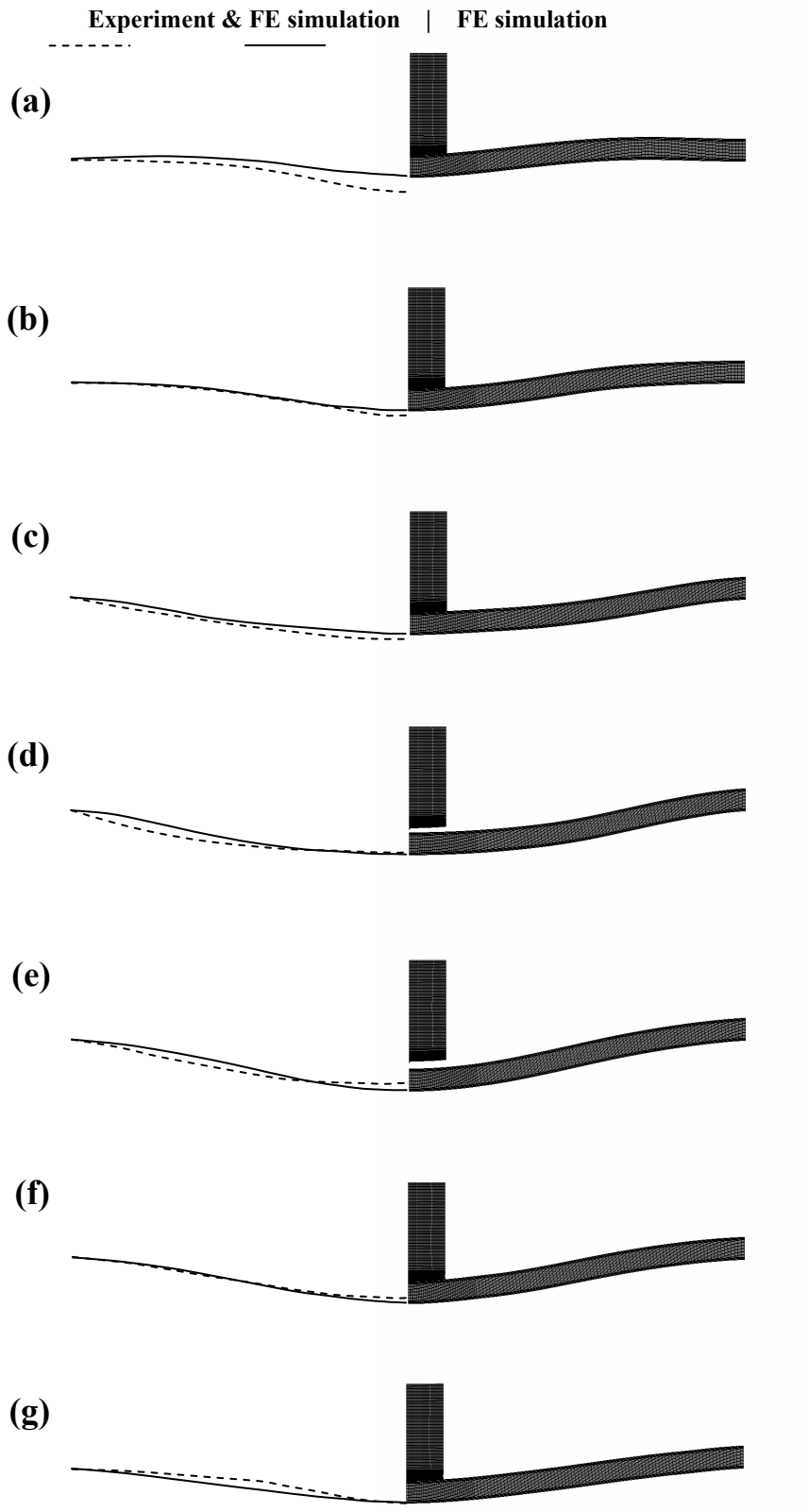

Fig. 4

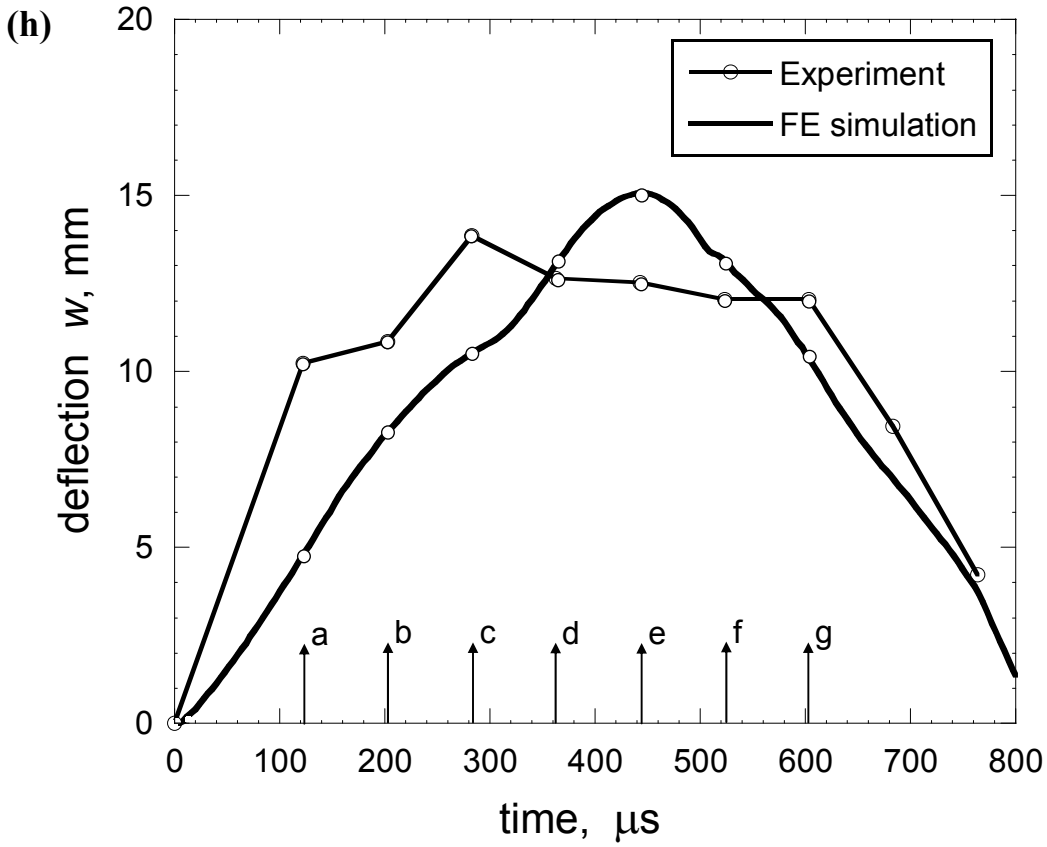
(h)
Experiment
FE simulation
deflection w, mm
time, μs
a
b
c
d
e
f
g
0
5
10
15
20
0
100
200
300
400
500
600
700
800

Fig. 4

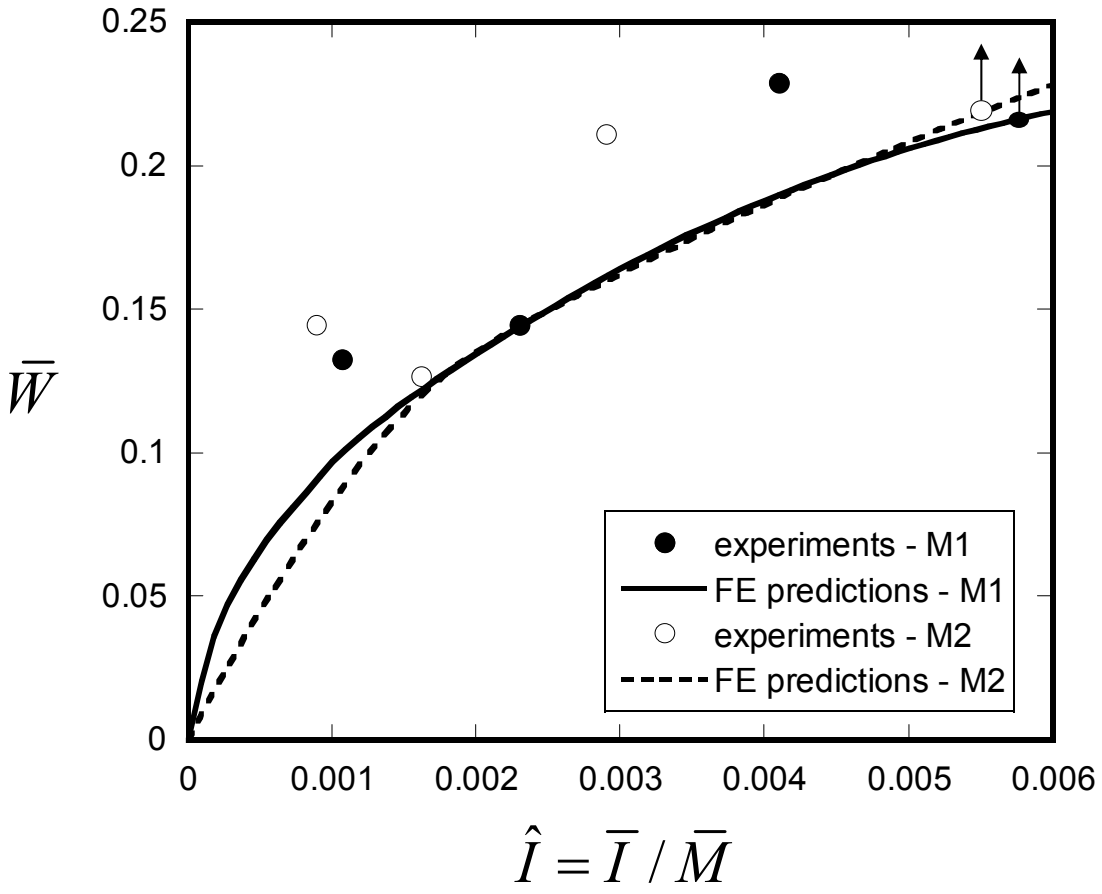
0.25
0.2
0.15
0.1
0.05
0
$\bar{W}$
0
0.001
0.002
0.003
0.004
0.005
0.006
$\hat{I} = \bar{I} / \bar{M}$
experiments - M1
FE predictions - M1
experiments - M2
FE predictions - M2

Fig. 5

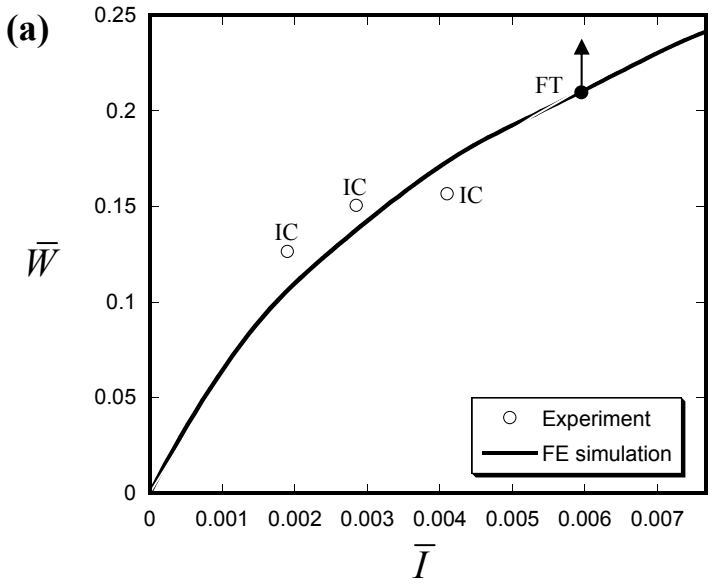
(a)
0.25
0.2
0.15
0.1
0.05
0
$\overline{W}$
FT
IC
IC
IC
Experiment
FE simulation
0
0.001
0.002
0.003
0.004
0.005
0.006
0.007
$\overline{I}$

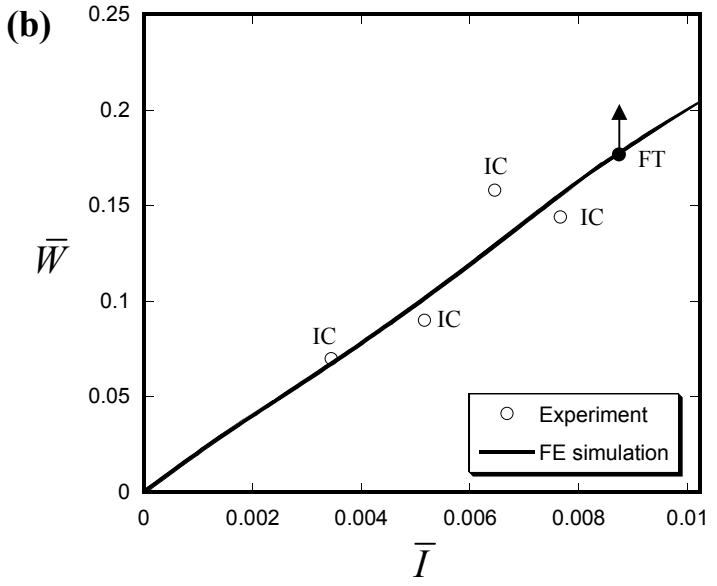
(b)
0.25
0.2
0.15
0.1
0.05
0
$\overline{W}$
IC
FT
IC
IC
IC
Experiment
FE simulation
0
0.002
0.004
0.006
0.008
0.01
$\overline{I}$

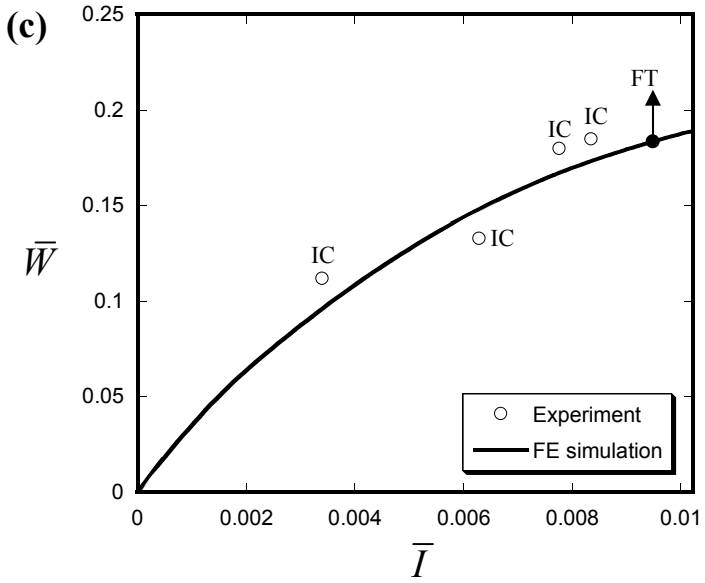
(c)
0.25
0.2
0.15
0.1
0.05
0
$\overline{W}$
FT
IC
IC
IC
IC
Experiment
FE simulation
0
0.002
0.004
0.006
0.008
0.01
$\overline{I}$

Fig. 6

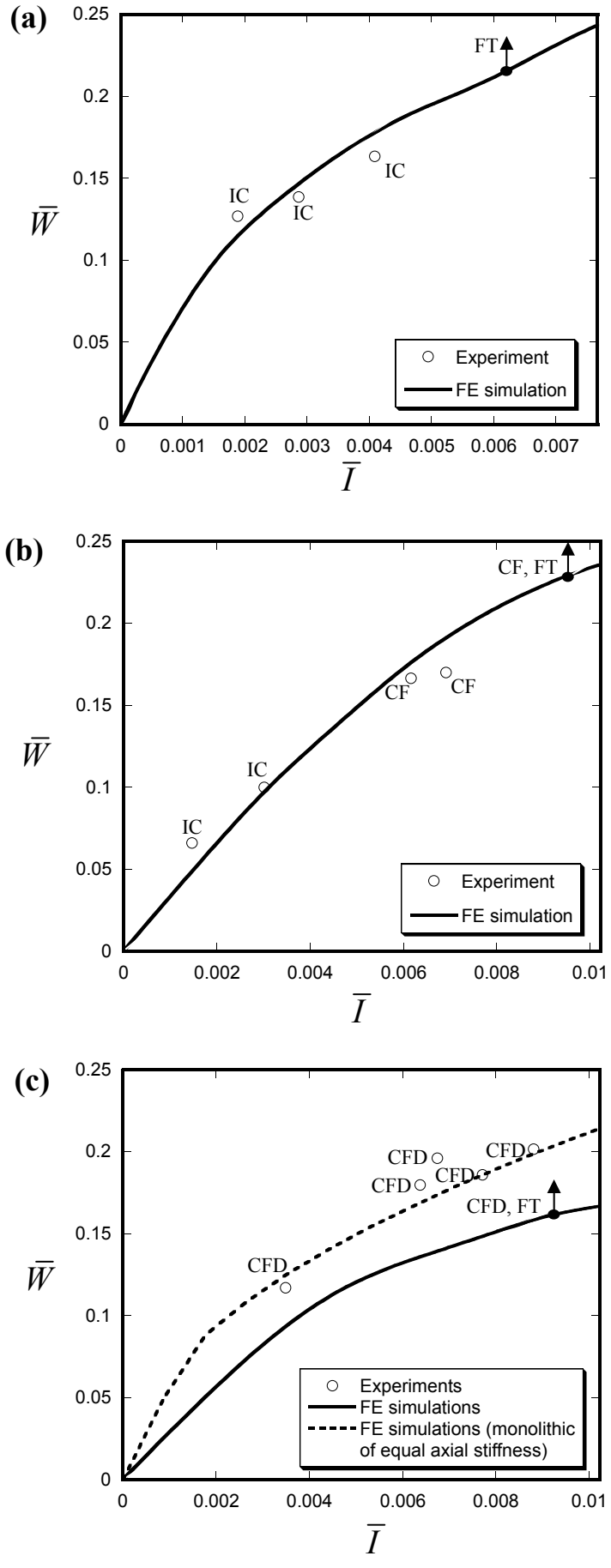
(a)
FT
IC
IC
IC
Experiment
FE simulation
$\bar{W}$
$\bar{I}$
(b)
CF, FT
CF
CF
IC
IC
Experiment
FE simulation
$\bar{W}$
$\bar{I}$
(c)
CFD
CFD
CFD
CFD
CFD, FT
CFD
Experiments
FE simulations
FE simulations (monolithic of equal axial stiffness)
$\bar{W}$
$\bar{I}$

Fig. 7

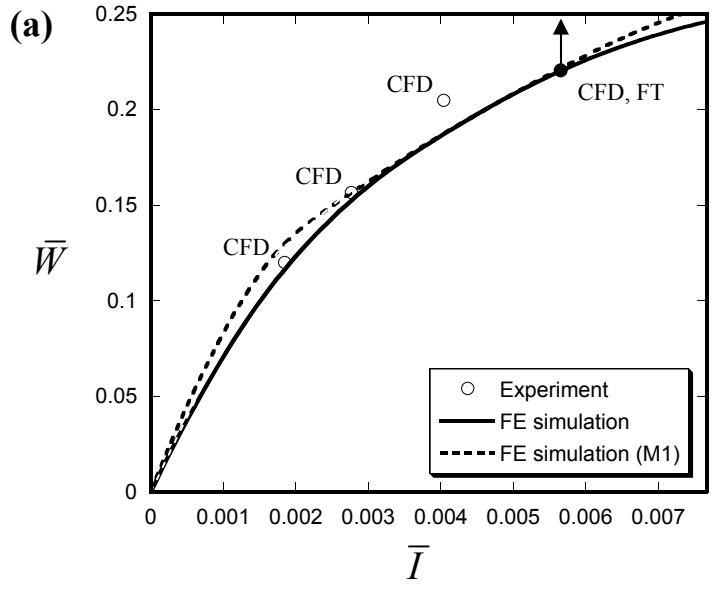
(a)
0.25
0.2
0.15
0.1
0.05
0
$\overline{W}$
CFD
CFD
CFD
CFD, FT
Experiment
FE simulation
FE simulation (M1)
0
0.001
0.002
0.003
0.004
0.005
0.006
0.007
$\overline{I}$

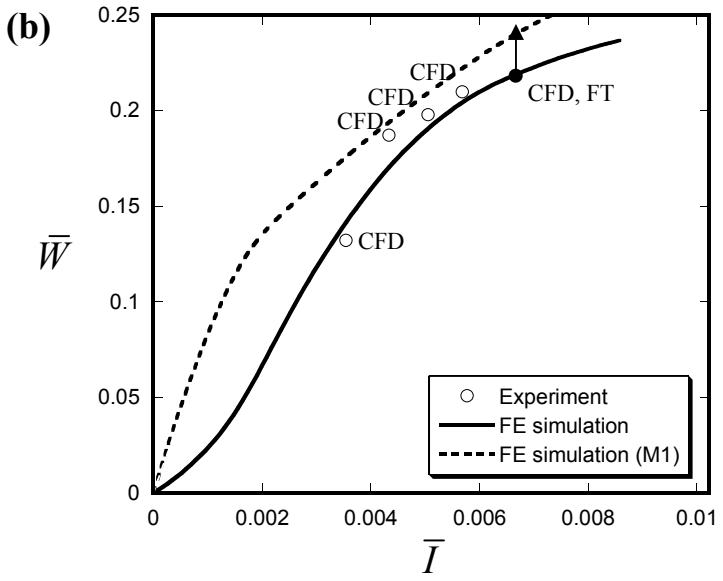
(b)
0.25
0.2
0.15
0.1
0.05
0
$\overline{W}$
CFD
CFD
CFD
CFD
CFD, FT
Experiment
FE simulation
FE simulation (M1)
0
0.002
0.004
0.006
0.008
0.01
$\overline{I}$

Fig. 8

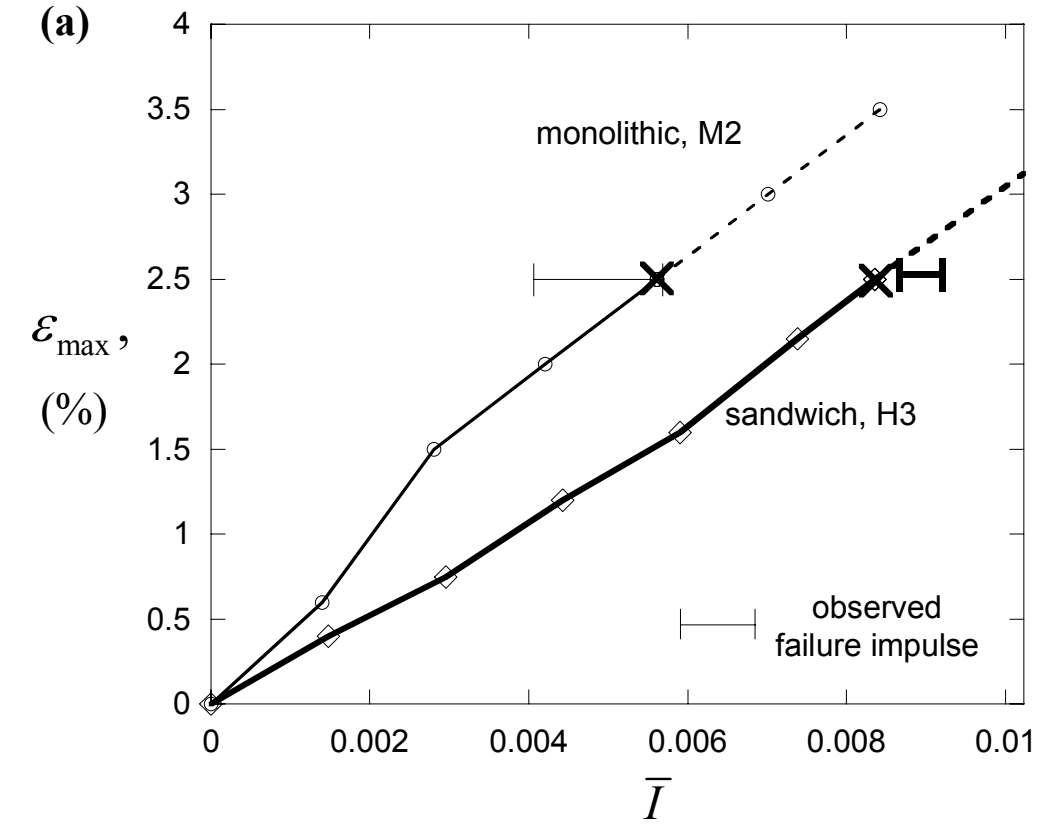
(a)
monolithic, M2
sandwich, H3
observed
failure impulse
ε_{max}, (%)
$\overline{I}$
0
0.5
1
1.5
2
2.5
3
3.5
4
0.002
0.004
0.006
0.008
0.01

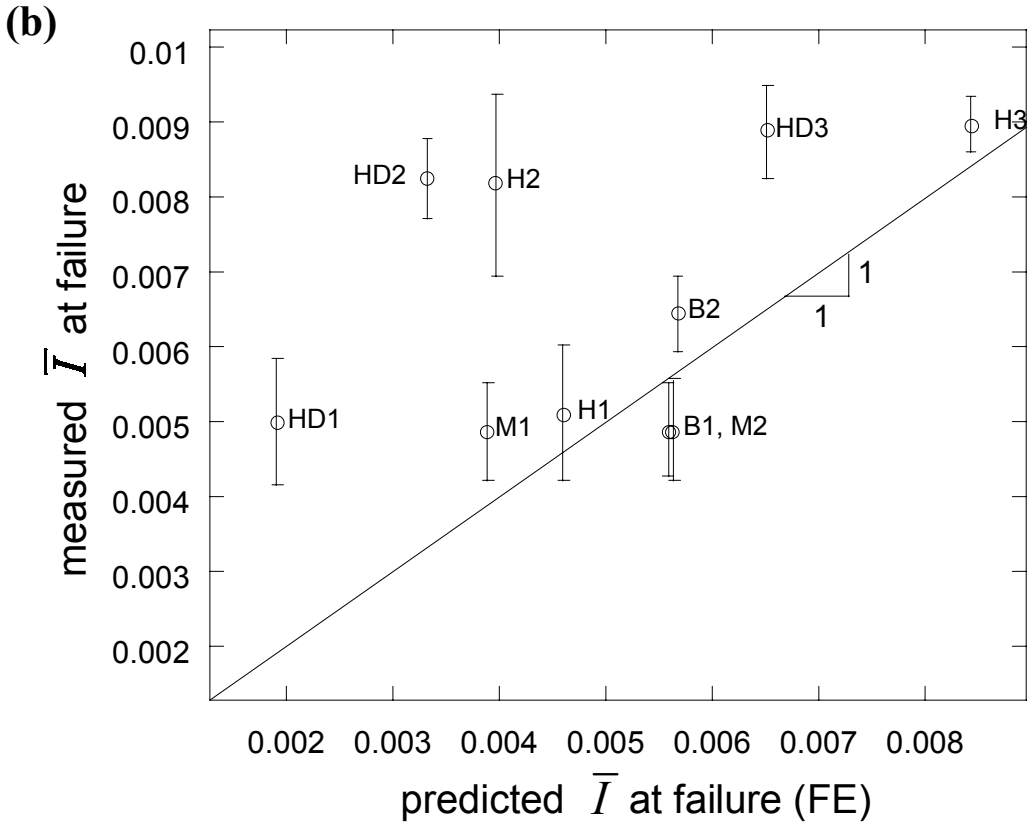
(b)
measured $\overline{I}$ at failure
predicted $\overline{I}$ at failure (FE)
HD1
HD2
H2
M1
H1
B2
B1, M2
HD3
H3
1
1
0.002
0.003
0.004
0.005
0.006
0.007
0.008
0.009
0.01

Fig. 9

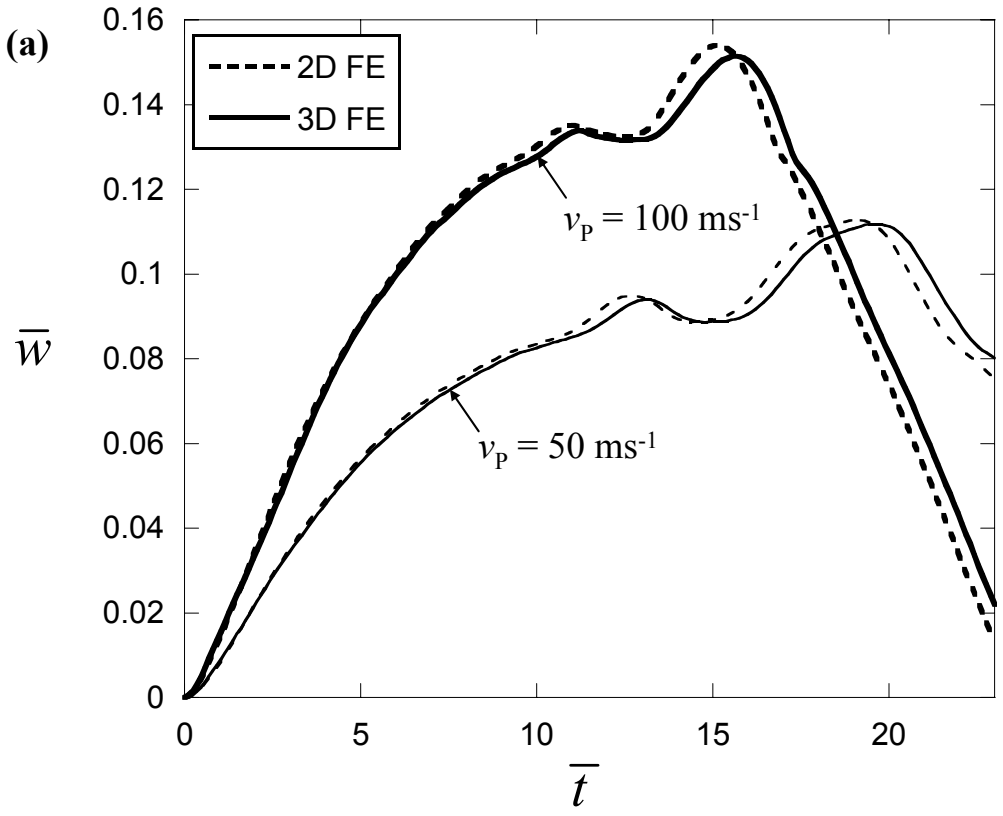
(a)
2D FE
3D FE
v_P = 100 ms^{-1}
v_P = 50 ms^{-1}
$\overline{w}$
$\overline{t}$
0.16
0.14
0.12
0.1
0.08
0.06
0.04
0.02
0
0
5
10
15
20

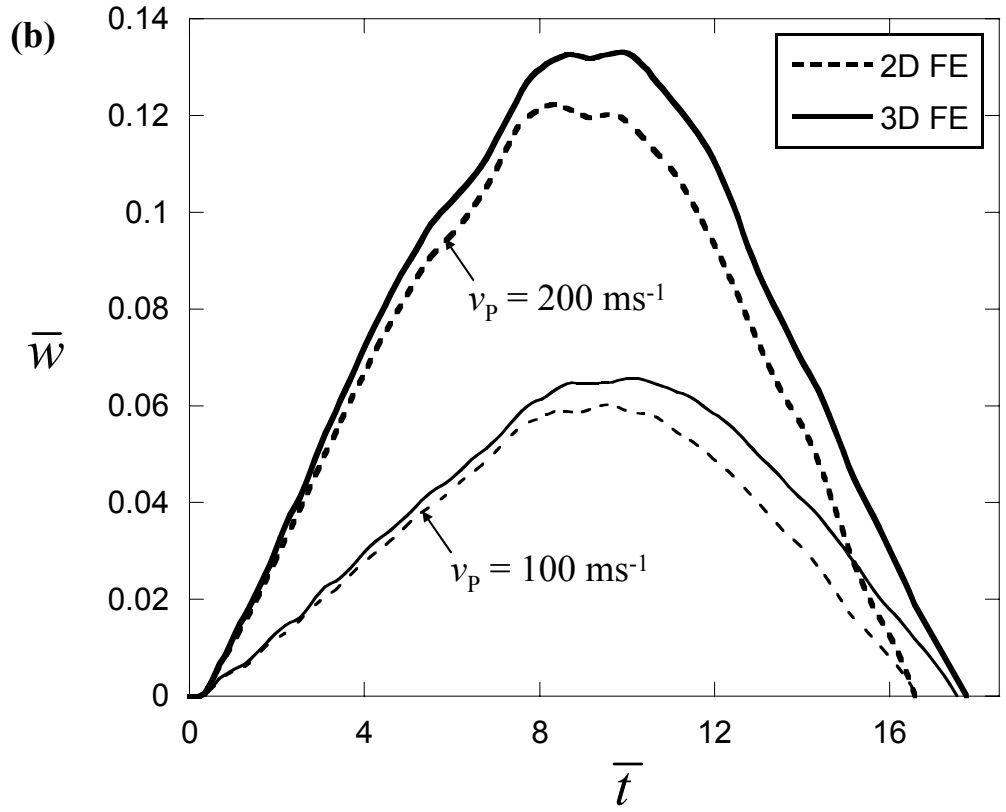
(b)
2D FE
3D FE
v_P = 200 ms^{-1}
v_P = 100 ms^{-1}
$\overline{w}$
$\overline{t}$
0.14
0.12
0.1
0.08
0.06
0.04
0.02
0
0
4
8
12
16

Fig. A1